NRC Research Press

ARTICLE

Long-term ice-rich permafrost coast sensitivity to air temperatures and storm influence: lessons from Pullen Island, Northwest Territories, Canada

H. Bay Berry, Dustin Whalen, and Michael Lim

Abstract: Response of erosive mechanisms to climate change is of mounting concern on Beaufort Sea coasts, which experience some of the highest erosion rates in the Arctic. Collapse of intact permafrost blocks and slumping within sprawling retrogressive thaw complexes are two predominant mechanisms that manifest as cliff retreat in this region. Using aerial imagery and ground survey data from Pullen Island, Northwest Territories., Canada, from 13 time points between 1947 and 2018, we observe increasing mean retreat rates from 0 ± 4.8 m a^{-1} in 1947 to 12 ± 0.3 m a^{-1} in 2018. Mean summer air temperature was positively correlated with cliff retreat over each time step via block failure ($r^2 = 0.08$; $p = 0.5$) and slumping ($r^2 = 0.41$; $p = 0.05$), as was mean storm duration with cliff retreat via block failure ($r^2 = 0.84$; $p = 0.0002$) and slumping ($r^2 = 0.34$; $p = 0.08$). These data indicate that air temperature has a greater impact in slump-dominated areas, whereas storm duration has greater control in areas of block failure. Increasingly, heterogeneous cliff retreat rates are likely resulting from different magnitudes of response to climate trends depending on mechanism, and on geomorphological variations that prescribe occurrences of retrogressive thaw slumps.

Key words: coastal erosion, permafrost, slope instability, arctic climate change.

Résumé : Les effets du changement climatique sur les mécanismes d'érosion sont de plus en plus préoccupants sur les côtes de la mer de Beaufort, lesquelles connaissent certains des taux d'érosion les plus élevés de l'Arctique. L'effondrement de blocs de pergélisol intacts et l'affaissement à l'intérieur de complexes de dégel régressif sont deux mécanismes prédominants qui se manifestent par le recul des falaises dans cette région. À l'aide d'images aériennes et de données de levés au sol de l'île Pullen dans les Territoires du nord-ouest au Canada, à partir de 13 points temporels entre 1947 et 2018, nous observons une augmentation des taux de recul moyens de $0 \pm 4{,}8$ m/a en 1947 à $12 \pm 0{,}3$ m/a en 2018. La température moyenne de l'air en été a été positivement corrélée avec le recul des falaises à chaque étape temporelle par rupture de bloc ($r^2 = 0{,}08$; $p = 0{,}5$) et par affaissement ($r^2 = 0{,}41$; $p = 0{,}05$), de même que la durée moyenne de tempête avec le recul des falaises par rupture de bloc ($r^2 = 0{,}84$; $p = 0{,}0002$) et par affaissement. ($r^2 = 0{,}34$; $p = 0{,}08$). Ces données indiquent que la température de l'air a un impact plus important dans les zones

Received 28 January 2020. Accepted 13 October 2020.

H.B. Berry.* Geological Survey of Canada, Bedford Institute of Oceanography, 1 Challenger Drive, Dartmouth, NS B2Y 4A2, Canada; Dalhousie University, Department of Earth Sciences, 1459 Oxford Street, Halifax, NS B3H 4R2, Canada.
D. Whalen. Geological Survey of Canada, Bedford Institute of Oceanography, 1 Challenger Drive, Dartmouth, NS B2Y 4A2, Canada.
M. Lim. Northumbria University, Engineering and Environment, Ellsion Building, Northumberland Road, Newcastle upon Tyne NE1 8ST, UK.
Corresponding author: H.B. Berry (e-mail: bay.berry@uqar.ca).
*Present address: Université du Québec à Rimouski, Département de biologie, chimie et géographie, 300 allée des Ursulines, Rimouski, QC G5L 3A1, Canada.

d'affaissement, tandis que la durée des tempêtes a une plus grande incidence dans les zones de rupture de bloc. Des taux de recul des falaises de plus en plus hétérogènes sont probablement le résultat de différentes amplitudes de réponse aux tendances climatiques en fonction du mécanisme et des variations géomorphologiques qui prescrivent des épisodes de dégel régressif. [Traduit par la Rédaction]

Mots-clés : érosion côtière, pergélisol, instabilité de pente, changement climatique dans l'Arctique.

Introduction

The ice-rich nature of the Beaufort Sea permafrost coasts has contributed to widespread, rapid coastal retreat. Even with the processes that drive erosion in this setting being restricted to the few open-water months each year (Aré et al. 2008), the reported mean coastal retreat rate for most areas of the Canadian Beaufort Sea in the late 20th and early 21st century was 1 m a^{-1}, with some locations experiencing upwards of 20 m of retreat in a single season (Table 1; Harper 1990; Solomon 2005; Radosavljevic et al. 2016).

Ground ice in permafrost soils may be present as pore ice, take the form of lenses, veins, or massive ice bodies, or comprise its own stratigraphic unit below the upper layer of sediment (Mackay 1972; Murton et al. 2004). Although ground ice meltwater provides a medium of downslope transport for eroded soil constituents, the high ice content of the permafrost also means that only a fraction of the volume of eroded material contributes to the nearshore sediment budget (Dallimore et al. 1996; Kokelj et al. 2009*b*). Indeed, the Mackenzie River has been estimated to contribute approximately 10 times more sediment annually to the Canadian Beaufort Sea than coastal erosion (Rachold et al. 2000). The rate and variability of coastal erosion in the Canadian Beaufort Sea is affected by intrinsic factors, including ground material, ground-ice and permafrost occurrence, and coastal geomorphology, and by extrinsic variables, such as storm intensity and sea ice occurrence as controlled by atmospheric and hydrodynamic forcing (Solomon 2005; Manson and Solomon 2007).

Increased retrogressive thaw slump (RTS; or "retrogressive thaw failure"; Couture et al. 2015) activity since the 1950s has been observed on the western Beaufort Sea coast; these features are characterized by rapid local headwall retrogression due to exposed ground ice melt, creating bowl-shaped structures with steep headwalls of exposed ice-rich permafrost and thawed sediments in the slump floor (Burn and Lewkowicz 1990; Lantuit and Pollard 2008; Ramage et al. 2017). The RTS morphology is in contrast to slumping coastal cliffs, which are also eroded via the thaw-related downslope mobilization of frozen ground material (Lantuit and Pollard 2005). However, where ground ice content of the cliff face is relatively homogeneous across long stretches, there is a similarly uniform rate of retreat that results in straighter cliff lines (Fig. 1). Retreat in an RTS, however, occurs from a point where massive ground ice is exposed, at a rate that is faster than the retreat of the adjacent cliffs.

Coastal retreat has implications from a terrain-loss perspective and for its potential chemical and atmospheric impact. The regression of coastlines, resulting in highly disturbed terrain or mobilization of ground material to the nearshore, impinges on sensitive regions such as terrestrial ecosystems (Environment Canada 2014), infrastructure and cultural sites of coastal communities (Mackay 1986), and industrial infrastructure and waste storage sites (Kokelj and GeoNorth Ltd 2002). Knowledge of erosive processes, trends, and future threats is integral to predicting the future viability of the region as a subsistence-use region, and for any potential infrastructure or hydrocarbon development.

In addition to physical threat to terrestrial systems and land-use, coastal retreat of permafrost cliffs also acts as a store of organic carbon, which may be liberated to the marine environment and to the atmosphere (Hugelius et al. 2014). Organic carbon stored

Table 1. Summary of annual coastal retreat rates for the Canadian Beaufort Sea–Mackenzie Delta region over the period of 1972 to 2000 reported by Solomon (2005).

Region	Mean (m a^{-1})	Standard deviation (m a^{-1})
Outer Mackenzie Delta	1.77	1.82
East Richards Island	0.4	0.62
Outer Mackenzie Delta Islands	1.51	2.79
West Richards Island	0.46	0.79
Tuktoyaktuk Peninsula	0.75	1.28

Fig. 1. (A) Oblique view of an active retrogressive thaw slump (RTS), stable RTS, and slumping coastal cliffs on Pullen Island, Northwest Territories (imagery courtesy of the Geological Survey of Canada, unpublished data, 2018. Visualized using Esri ArcScene v.10.5). (B) Active, partially stable, and stable RTS occurrences in the Mackenzie Delta region of the Canadian Beaufort Sea coast. (Point data from Couture et al. 2015; base data from Statistics Canada 2016*a*, 2016*b*. Visualized using Esri ArcMap v.10.5.).

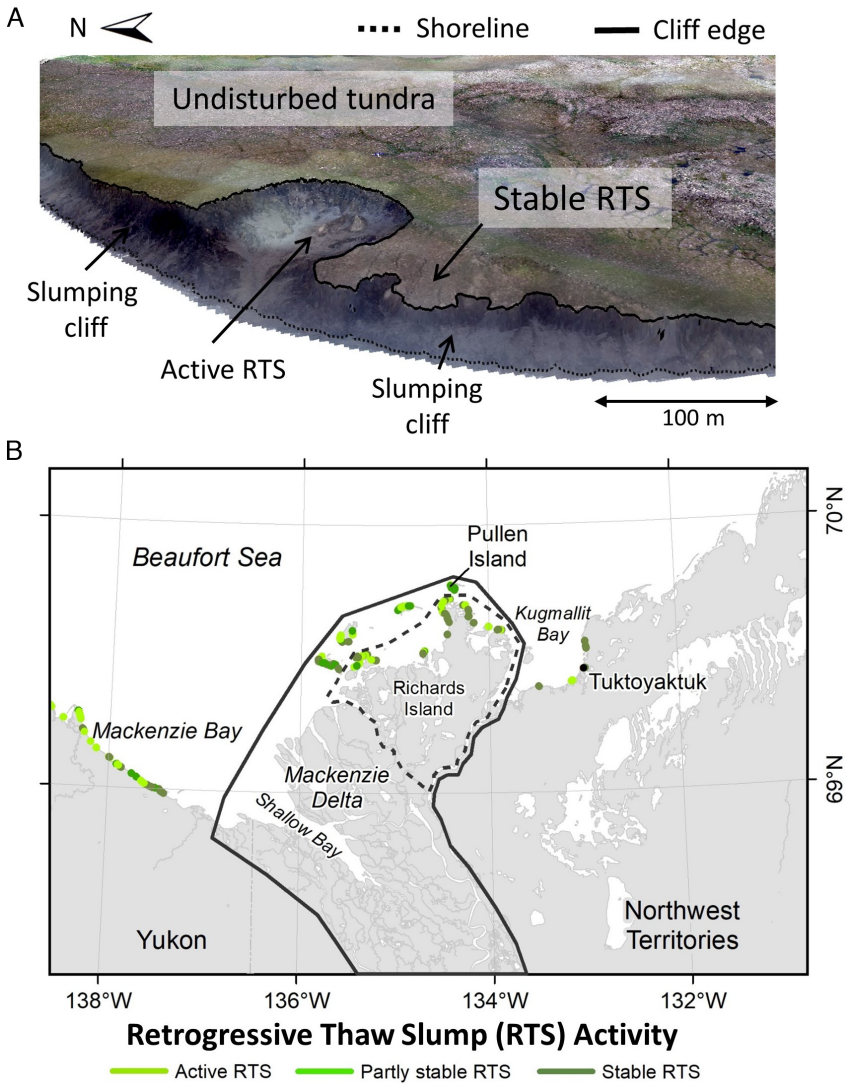

Fig. 2. Location of Pullen Island on the Mackenzie Delta, Northwest Territories (Aerial imagery courtesy of the Geological Survey of Canada, unpublished data, 2018; and base data from Statistics Canada 2016*a*, 2016*b*. Visualized using Esri ArcMap v.10.5.).

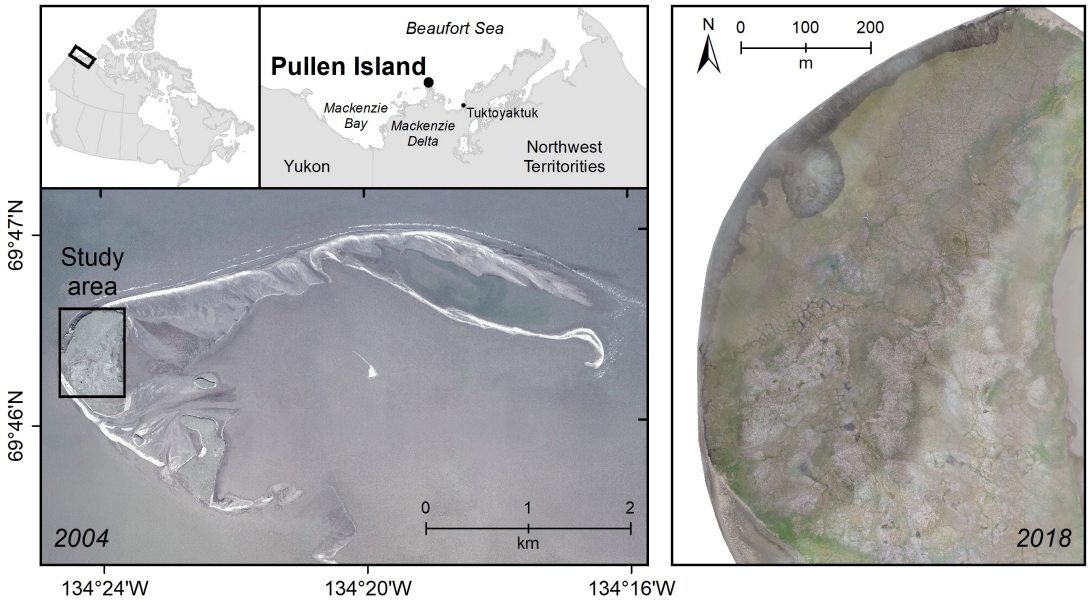

in the upper layers of sediment that is remobilized during erosion of ground material may be accumulated on the slope or shore, be incorporated into the nearshore sediment budget along with nitrogen and nutrient soil components, or can be released to the atmosphere by microbial mineralization (Cassidy et al. 2016; Tanski et al. 2017). Although the amount of carbon dioxide released to the atmosphere is small in magnitude, it may be enough to offset the carbon sequestration of undisturbed tundra in the same region, resulting in a net positive contribution over the course of a growing season (Cassidy et al. 2016).

Pullen Island, on the outer Mackenzie Delta, Northwest Territories (Fig. 2) has been observed intermittently for over seven decades, via aerial photography and ground surveys. The island's western cliffs are eroding via slumping and block failure (Couture et al. 2015), which is occurring over a relatively small area that is uniformly subject to extrinsic environmental conditions. These long-term observations and the ability to differentiate erosion mechanisms affords an opportunity to assess specific geomorphic responses under recent changes in mean annual temperatures and storm intensities. We analyzed erosion processes resulting in cliff retreat, and sensitivities to summer air temperatures and storm events to investigate future trends under warming Arctic temperatures. Aerial imagery and ground survey data from 1947 to 2018 were used to determine cliff position and the dominant mechanism resulting in cliff retreat. Weather data from the Environment and Climate Change Canada station at Tuktoyaktuk were available from 1958 to 2018. Due to differences in measurement frequency, the study period used for regressions of weather and cliff retreat was 1967–2018. Ultimately, the purpose of this study was to investigate the relationship between two extrinsic environmental conditions during the erosion season (summer air temperature and storm duration) and cliff retreat on Pullen Island, in terms of rate and mechanism.

The definition of "coastline" for this type of study is variable in the literature — broadly speaking, this can be any visually discernable line that separates the terrestrial and marine

environments (Boak and Turner 2005), and examples include the wet-dry line (e.g., Solomon 2005), the slope base (e.g., Harper 1978), the cliff edge (e.g., Solomon et al. 1994), or the vegetation line (e.g. Cunliffe et al. 2019). As such, in addition to cliff line retreat, this study also addresses two other possible measures of coastal change: shoreline and volumetric change. Although in some areas, the use of these different lines may yield similar measurements (such as very steep cliffs where the cliff edge and base of slope are inseparable in aerial imagery), these variable measures may have different implications depending on the slope morphology or the focus of the analysis (e.g., terrain loss versus sediment transfer, or marine impacts versus land use). To assess the differences in potential analytical results, "shoreline" retreat was assessed at the base of the slope in addition to the cliff retreat measurement (Fig. 1), as well as the change in volume of material based on digital surface models (DSMs) generated by photogrammetry of imagery from 1992, 2016, 2017, and 2018.

Methods

Study area

Pullen Island, Northwest Territories, is part of the Mackenzie Delta on the Beaufort Sea shelf (Fig. 2). The island is composed of tundra uplands and dynamic sand spits. The focus of this study is the west-facing ice-rich cliff; the eroding area includes near-vertical tundra cliffs failing through block collapse, slumping coastal cliffs, and RTSs (Couture et al. 2015). There are no in-depth reports on the state of cliff retreat on Pullen Island, although it has been included in a multi-site publication of Mackenzie Delta stratigraphy (Murton et al. 2004), and there are many reports of permafrost geomorphology and coastal processes in the Mackenzie Delta–Beaufort Sea region (e.g., Harper et al. 1985; Baird and Associates 1995; Taylor et al. 1996; Solomon 2005; Couture et al. 2015).

As Pullen Island lies within the continuous permafrost zone, the ground below a certain depth remains frozen throughout the year. The island has a maximum elevation of 26 m at the top of the west-facing cliffs and is marked by ice-wedge polygon networks. The upper layer of material that thaws seasonally is termed the active layer; this material is generally thought to be most susceptible to erosion in the summer months (Aré et al. 2008). The thickness of the active layer is inherently linked to summer temperatures, which affect the depth to which the ground thaws.

Murton et al. (2004) identified two stratigraphic units on Pullen Island, accounting for the upper 16 m: sandy silt and massive ice. The sediment unit is approximately 12 m thick, and includes unlithified sandy silt, fine sand, and few pebbles to cobbles that are interpreted to have been brecciated subglacially at the margin of the Laurentide Ice Sheet, in addition to ice veins and blocks. The massive ice unit is at least 4 m thick and is interpreted as buried basal ice (Murton et al. 2004). The contact between the sediment unit and the underlying massive ice is an angular unconformity. Ground ice, as blocks and wedges, is visible in the cliff face. The west-facing cliff has been visually classified as having high ice content (>75%; Couture et al. 2015).

Generation of digital surface models

Unmanned aerial vehicle (UAV)-based imagery from 2016, 2017, and 2018 was processed using Pix4Dmapper photogrammetry software to produce georeferenced DSMs and aerial imagery mosaics, which were georeferenced using ground control points measured during each survey. The DSMs are generated based on the structure-from-motion theorem (Ullman 1977, 1979), which states that the three-dimensional structure of an object can be interpreted from at least four points seen from a minimum of three different viewing angles. The multiple perspectives required for this technique are provided by overlapping photographs, which show the same area on the ground from different angles.

Table 2. Resolution and root mean square (RMS) positional error of aerial imagery relative to 2018 imagery.

Year	Pixel size (m)	RMS positional error (m)
1947	1.35	6.09
1950	1.29	5.14
1967	1.29	4.09
1974	1.88	4.55
1985	4.67	7.87
1992	0.25	2.45
2004	0.5	1.76
2016	0.025	0.48
2017	0.025	0.29
2018	0.025	—

In addition to the UAV-derived models, a DSM was generated using historical aerial photographs from 1992. Two flight lines of overlapping photographs had been collected over the study area, allowing multiple perspectives of points on the ground and for the generation of a DSM from seven images following the structure-from-motion principles. This model was also created using Pix4Dmapper software and was scaled and georeferenced using 16 ground control points taken from the 2018 imagery and DSM, based on landmarks that were visible in the imagery from both years. The quality of lateral georeferencing for this model (and all imagery included in the analysis) is described in Table 2 by the root-mean square positional error relative to the 2018 UAV imagery.

The ability of the photogrammetry software to calculate the vertical component of the 1992 DSM was assessed by comparing it to the inland elevation shown in the UAV models, assuming little vertical ground motion of the undisturbed tundra. Some minor difference should be expected based on annual variations of active layer thaw depth and associated subsidence, as well as differences in vegetation growth. However, when elevation profiles drawn perpendicular to the cliff are compared, there was a vertical offset of −3.1 to 2.3 m between the 2018 and 1992 DSMs on the inland end of the transects. Coarse vertical corrections were made over linear swaths of the 1992 DSM to better align the inland region of the 1992 DSM with the 2018 DSM. The sections for adjustment were drawn from transect lines extending from an inland baseline at 30 m intervals, and elevation profiles drawn down the center of each section were measured on the 1992 and 2018 DSMs (Fig. 3B). A constant value equal to the difference in elevation at the inland end of the profile was then added to each cell within the section on the 1992 DSM (Fig. 3D). The adjusted sections were compiled to a single raster, and this adjusted DSM was used for the subsequent volume calculations and elevation profiles (Fig. 3C). Prior to this adjustment, the difference in elevation between the undisturbed tundra areas of the 1992 and 2018 DSMs had a mean of −1.05 m and standard deviation of 1.8 m; the adjusted DSM had a mean difference of 0.15 m and standard deviation of 1.2 m. When the other two UAV-derived models were compared with the 2018 DSM in the same area, the 2016 DSM had a mean vertical difference of 0.4 m and standard deviation of 0.2 m, and the 2017 DSM had a mean difference of 0.06 m and standard deviation of 0.48 m.

Coastline digitization

Coastlines were identified based on slope morphology; the “cliff line” being the upper edge of the slope and the “shoreline” being the base. The lines were digitized by hand in ArcMap for each year with available imagery and were drawn by a single user for consistency. In addition to the imagery collected by UAV, a greater temporal extent has been

Fig. 3. Coarse adjustment of the digital surface model (DSM) produced from 1992 historical aerial photographs based on inland elevations of the 2018 unmanned aerial vehicle-derived DSM. (A) The original DSM; (B) the location of elevation profiles used to compare the 1992 DSM to the 2018 DSM, with the example profile indicated in red; (C) the adjusted 1992 DSM; (D) An example of the comparison between elevation profiles being used to adjust the 1992 DSM, shown with 5× vertical exaggeration. (Visualized using Esri ArcMap v.10.5.).

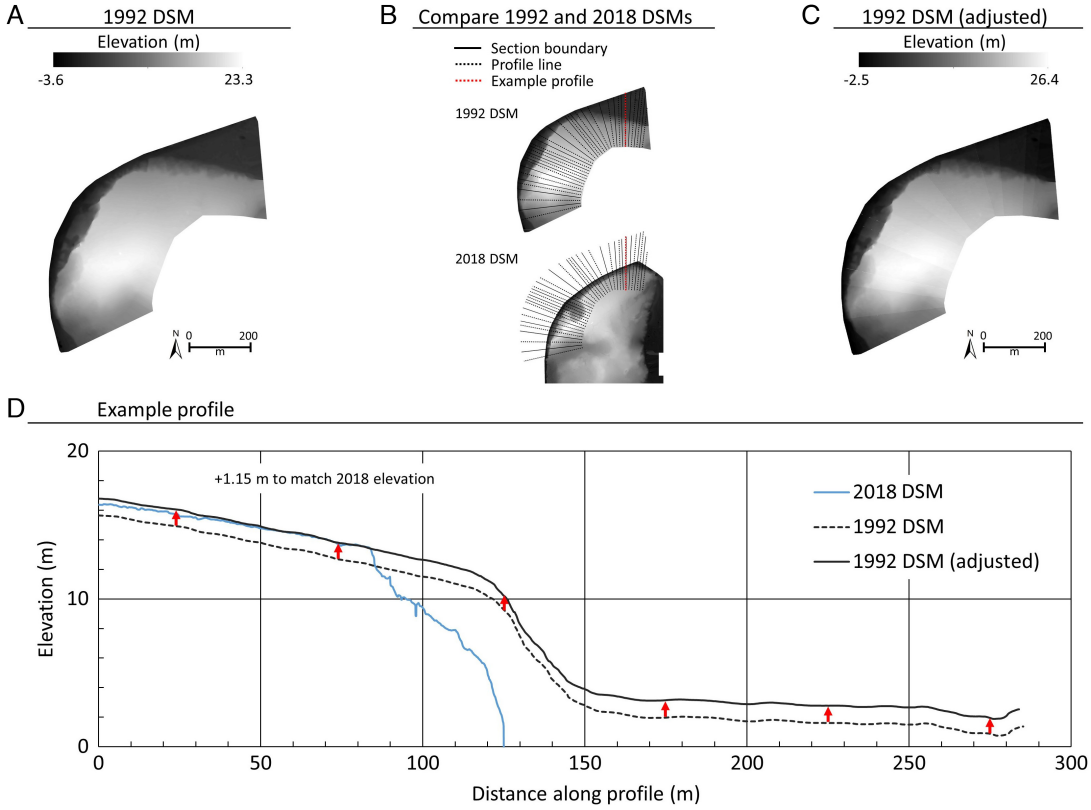

achieved using historical aerial photographs, although at the cost of resolution and positional referencing quality (Table 2). The photographs, obtained from Natural Resources Canada archives, were scanned at 600 dpi and georeferenced in ArcMap. The control points used were primarily located at ice-wedge intersections, referenced to the 2016–2018 imagery. Global positioning system points from ground surveys of the cliff line in 2013–2015 were converted to lines in ArcMap and compiled with the digitized cliff lines in a single shapefile (Fig. 4). Cliff and shorelines from a total of 13 years spanning 1947–2018, were included in the final calculations (Table 2).

The positional error of each image was measured relative to the imagery for 2018. Because cliff retreat was calculated as the relative change in cliff line position, the error in geographic position is less important to the measurement than error in registration between images. Thus, the error was measured as the distance between the registered location of the same feature on the image in question and the 2018 imagery when the two where overlain in a geographic information system. Where identifiable on the imagery, 26 points were chosen for validation, which were not used as georeferencing points in the registration of the imagery. Imagery from 1985 had the maximum root mean square (RMS) positional error recorded (7.87 m relative to the 2018 imagery). The coarse resolution

Fig. 4. Location of cliff and shorelines on Pullen Island, Northwest Territories, 1947–2018. Lines from 1950, 1967, 1974, 2013, 2014, 2015, and 2017 excluded for simplicity. Outlined are areas designated as dominated by slump or by block failure for erosion rate comparison. Oblique images show sections of (A) slumping coastal cliffs, (B) retrogressive thaw slumping, and (C) block failure, as seen in the 2018 3D model. (Imagery courtesy of the Geological Survey of Canada, unpublished data, 2018; plan view visualized using Esri ArcMap v.10.5, and oblique views using ArcScene v.10.5).

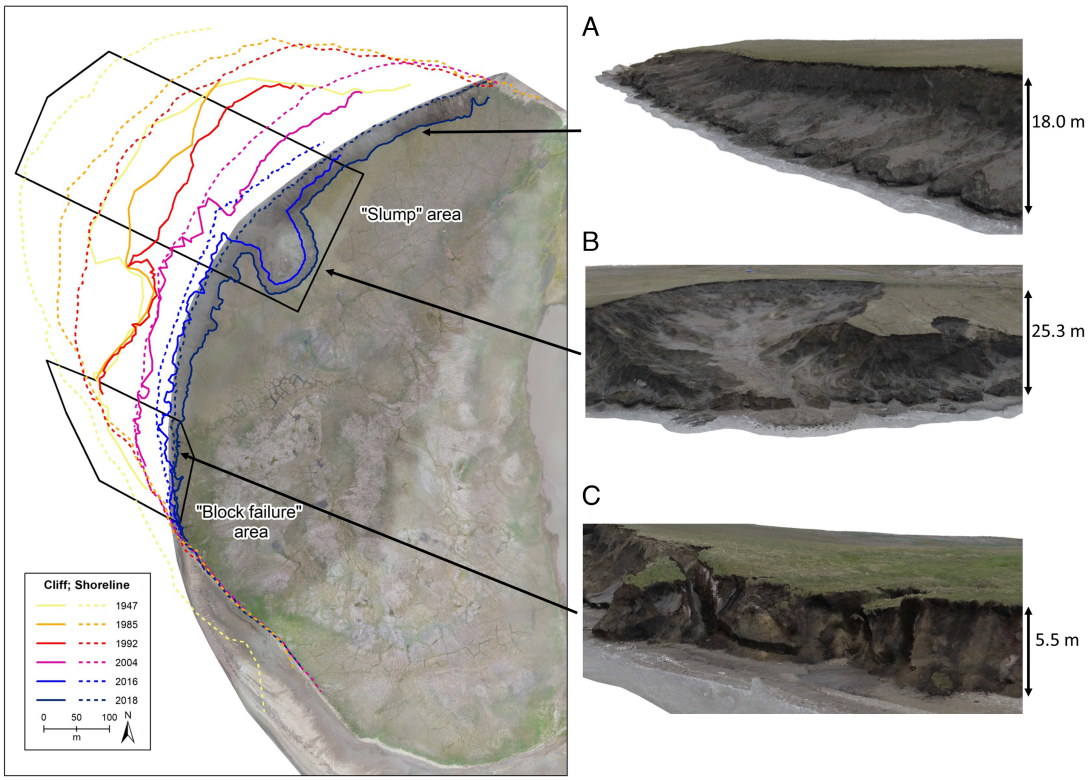

and low visual contrast of the 1985 imagery posed a particular challenge when locating control points for georeferencing as fewer landmarks (such as ice-wedge polygons) were visible.

For each year with imagery of sufficient resolution, sections of cliff were visually categorized as *clearly slumping*, *clearly block failure*, or *transitional*. Two areas were isolated for rate comparison; a section of cliff where the primary erosion mechanism is slumping, and a section dominated by block failure (Fig. 4). The cliff retreat rates were calculated for each period using transects that could be used to consistently compare both landward recession and form change through time.

Cliff retreat rate calculation

The digital shoreline analysis system (DSAS; Thieler et al. 2017), an extension for ArcMap, was used to calculate the rates of cliff line change. DSAS requires the user to input digitized cliff lines, over which transects are drawn from a user-defined baseline every 10 m. The system computes the distance between each point along a transect where it is intersected by a cliff line, and the positional difference between successive cliff lines can then be converted to mean annual retreat rates by dividing by the number of years between the two points. The mean rate was calculated for each pair of cliff-lines, and the mean annual values were used as the short-term rates. Three equal-interval periods (1947–1970, 1971–1994, and

1995–2018) were used for long-term rate calculations. Standard deviations have been calculated for each of the determined rates to represent the spatial variation occurring during each time period.

Volume change calculation

Volume change within the block failure and slump areas (Fig. 4) were calculated based on elevation differences of DSMs from 1992, 2016, 2017, and 2018. Positive and negative volume changes were calculated separately to differentiate areas of accretion or erosion of material, and then combined to find the net volume change. Due to the varying aerial coverage of the imagery and DSMs, the region identified as being primarily affected by block failure was represented only by very short sections in the UAV models, and by a varying amount for each year. To account for this inconsistency, the volume change values are reported as mean annual change in m^3 per 100 m of shoreline in the later year of the time step (i.e., for 2017–2018, the length of the 2018 shoreline is used). It is assumed that the trends in volume change that were calculated based on this small section are representative of the entire block failure area.

Air temperature and storms

Landfast ice (immobile sea ice that is fixed to the coast; Mahoney 2018) has historically been present in the region between February and June in the Mackenzie Delta region, and there appears to be a trend of later onset of landfast ice formation by approximately 2.80 weeks per decade (mean formation and breakup for 1983–2009; Galley et al. 2012). Considering the presence of pack ice, the traditional open-water seasons have typically been between July and September (Solomon 2005). The presence of sea ice up to the shore limits thermal erosion by wave action, so analysis was restricted to the open-water season (Aré et al. 2008; Wobus et al. 2011). For this analysis, the open-water season for inclusion of storm events was maintained as July to September; however, it should be noted that some events outside of this period that could have impacted coastal retreat rates may have been excluded in the case of longer open-water periods in a given year.

Wind and air temperature data from the Environment and Climate Change Canada weather station in Tuktoyaktuk, Northwest Territories, for the 1958–2018 open-water seasons (July, August, and September) were processed using methods adapted from Atkinson (2005). Data were collected every 6 h between 1958 and 1992, and hourly between 1993 and 2018. The data set contained occasional gaps of ≤5 h, approximately 30 gaps of 6–24 h, and eight gaps of >24 h. The missing times were excluded from the analysis, although we acknowledge that this may have resulted in missed or underestimated duration of storm events due to broken continuity of the record.

Storms were defined as events with wind speeds of at least 10 m s^{-1} sustained over at least 6 h. These were filtered for events that would affect the actively eroding side of Pullen Island; storms with onshore wind directions between 270° and 15° from the north. "Synoptic duration" was calculated as the time between the first and last recorded wind speeds exceeding 10 m s^{-1} for each event. "Core duration" was calculated as the time during which wind speed was in the upper 50th percentile for each event. An example of the threshold wind speeds for a single event are shown in Fig. 5 to illustrate the definition of these storm duration values. The average synoptic and core durations and the mean air temperature have been calculated for every year on record. A five-year moving average was calculated for each metric, and linear regressions (date against storm duration and date against temperature) were calculated using these averages to assess weather trends over the period of observation.

Fig. 5. An example storm event (18–21 July 2016; data retrieved from Environment and Climate Change Canada 2016) to illustrate threshold wind speeds in definition of synoptic and core storm duration. The entire storm event is contained within the blue box, the length being equal to the synoptic duration. Periods during which the wind speed is equal to or greater than the median speed for the event, highlighted in yellow, are counted into the core duration. Adapted from Atkinson (2005).

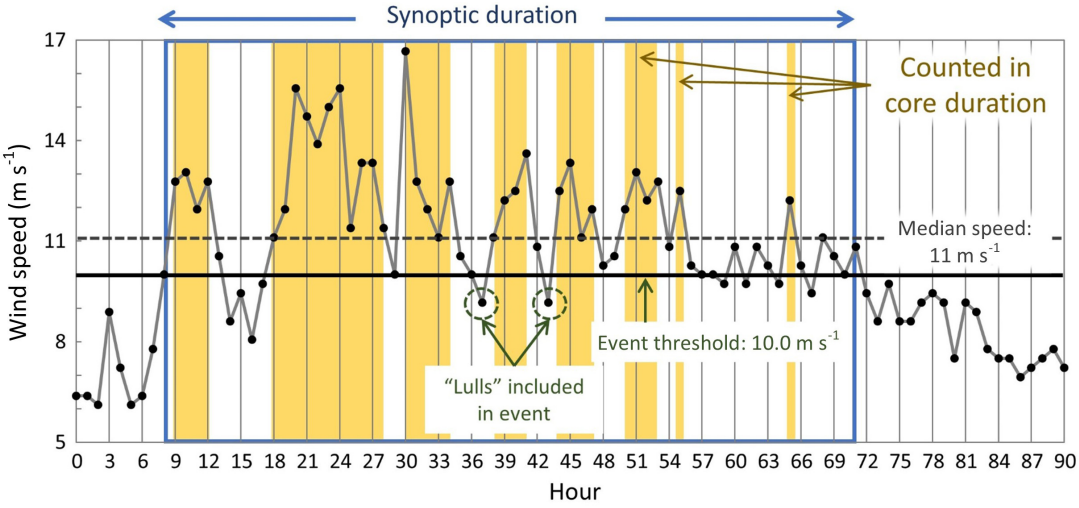

Satisfaction of the assumptions of linear regression was assessed for each of the dependent variables (cliff retreat across the study area, in the block failure area, and in the slump area) and independent variables (air temperature and core storm duration). Observations are independent from one another; the values used for each data point represent discrete periods of time. The independent variables are normally distributed. Although the rates of cliff retreat in the slump area and over the entire study area are moderately left-skewed and the rates of retreat in the block failure area are severely right-skewed (skew coefficient of 1.3), the regressions do not exhibit heteroscedasticity when residuals are plotted against predicted values. As such, linear regression is considered acceptable for our purposes.

The mean cliff retreat rates for the entire study area and for each of the block failure and slump areas were regressed against mean air temperature and mean core storm duration. For this calculation, the mean weather metrics for the entire time step was compared with the annual rate of retreat. For example, the mean air temperature for all of 1967–1974 was used as the *x*-value to the mean retreat rate in the slump area for this period. Similar regressions were also calculated for mean air temperature and mean core duration against the mean retreat in the entire study area. For each regression, coefficients of determination (r^2) and probability values (p) were calculated, to comment on the significance of the observed relationships. Note that because weather data begin at 1958 and the next available imagery was from 1967, the first time interval for the long-term comparison only represents the step from the 1967 to 1974 imagery.

Results

The mean annual rate of cliff retreat, calculated over the entire study area, shows a three-phase increase: rising by 0.53 m a^{-1} $decade^{-1}$ (1947–1985), through 1.8 m a^{-1} $decade^{-1}$ (1985–2013) to an increase of 1.6 m a^{-1} (2013–2018; Fig. 6A). The range of rates experienced across the study area also increased over time (Fig. 6B). Certain areas, such as the

Fig. 6. Mean annual erosion rates on Pullen Island, Northwest Territories, 1947–2018. (A) Mean cliff line erosion rate of the entire study area. Horizontal error bars are proportional to the number of years over which the measurements are averaged, and vertical error bars are proportional to the positional error of the source data. (B) Mean, maximum, minimum, and standard deviation of the annual cliff erosion rates for the entire study area. (C) Mean rate of cliff retreat in the slumping and block failure areas. (D) Mean shoreline erosion rate of the entire study area. Horizontal error bars are proportional to the number of years over which the measurements are averaged, and vertical error bars are proportional to the positional error of the source data. (E) Mean, maximum, minimum, and standard deviation of the annual shoreline erosion rates for the entire study area. (F) Mean rate of shoreline retreat in the slumping and block failure areas.

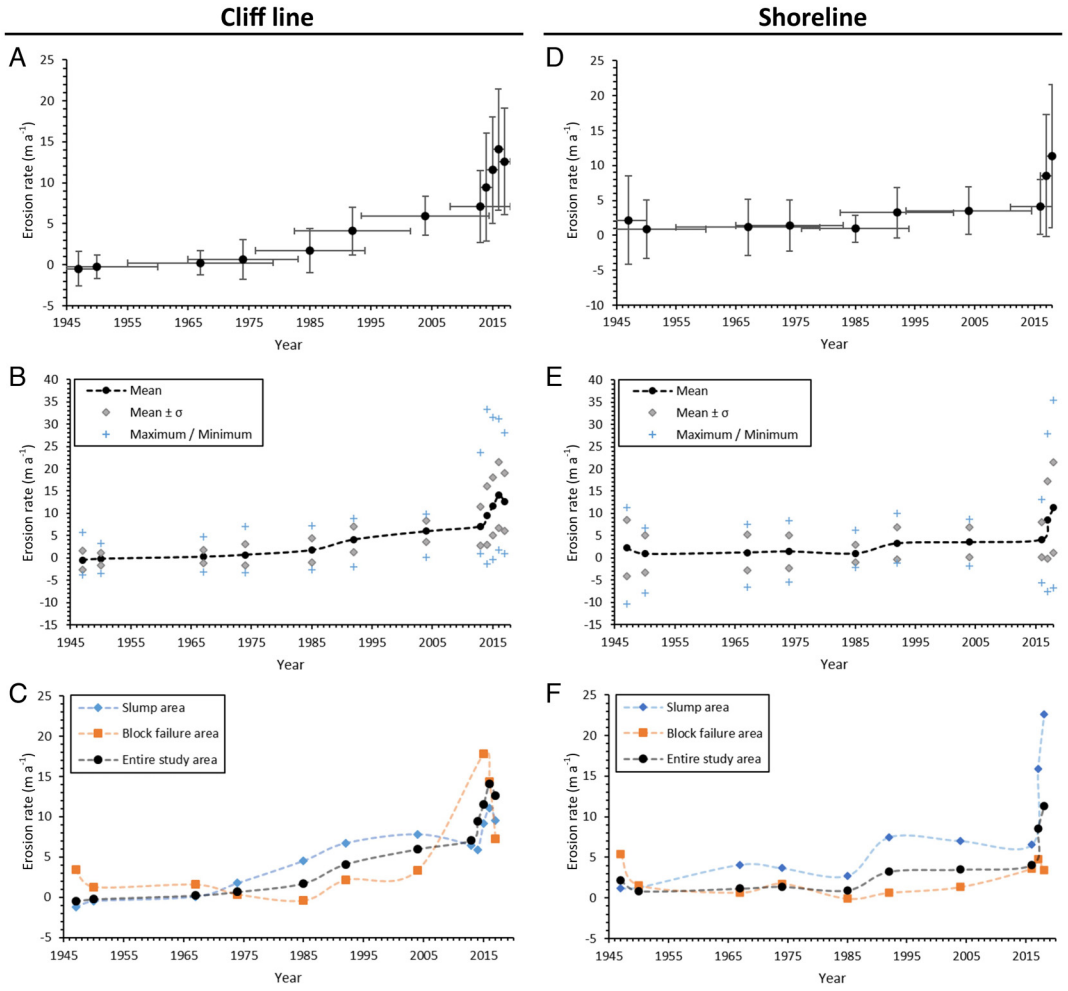

west-facing cliff section, maintained a more consistent rate of change throughout the study period, whereas others experienced more dramatic increases in cliff retreat rates (Fig. 7). The mean retreat rates were broken down into two categories based on failure mechanism, namely "block failure" areas and "slump" failure areas (Fig. 6C). Although equal within one standard deviation to the mean cliff retreat rates for the corresponding time period, shoreline retreat rates show a more gradual trend over time: decreasing slightly by 0.15 m a^{-1} $decade^{-1}$ (1947–1985), then rising by 1.2 m a^{-1} $decade^{-1}$ (1985–2004), followed by 3.9 m a^{-1} $decade^{-1}$ (2004–2018; Fig. 6D). There was an overall increase in range of shoreline retreat rates across the study area (Fig. 6E); however, when divided by failure mechanism, the

Fig. 7. Mean rate of annual cliff retreat through time. Focusing on the northwest area of Pullen Island, mean rates for each time period (1947–1970, 1971–1993, 1994–2018) are displayed on an equal interval scale of 5 m a^{-1}. (Imagery courtesy of the Geological Survey of Canada, unpublished data, 2018. Visualized using ESRI ArcMap v.10.5.)

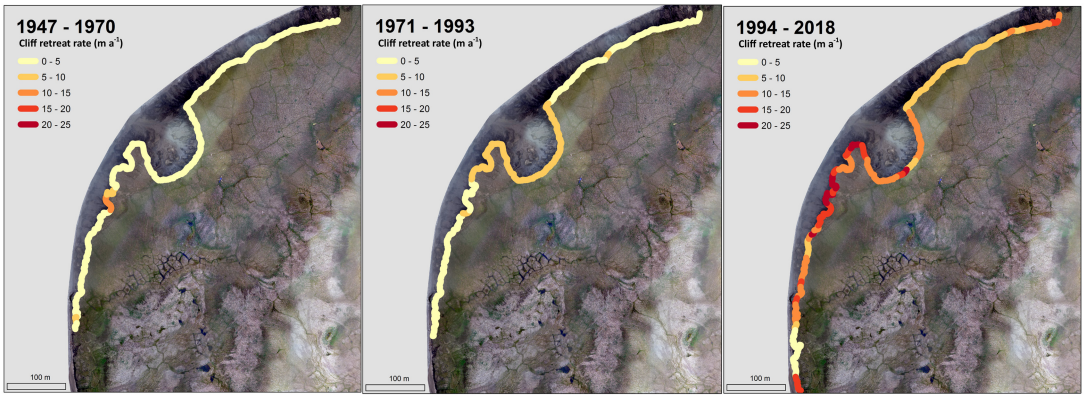

Fig. 8. Elevation difference between digital surface models over (A) 1992–2016, shown over imagery from 2016; (B) 2016–2017, shown over imagery from 2017; and (C) 2017–2018, shown over imagery from 2018. Positive values (blues) indicate increased elevation, and negative values (reds) indicate decreased elevation between the two years. (Imagery courtesy of the Geological Survey of Canada, unpublished data, 2016–2018; visualized using ESRI ArcMap v.10.5)

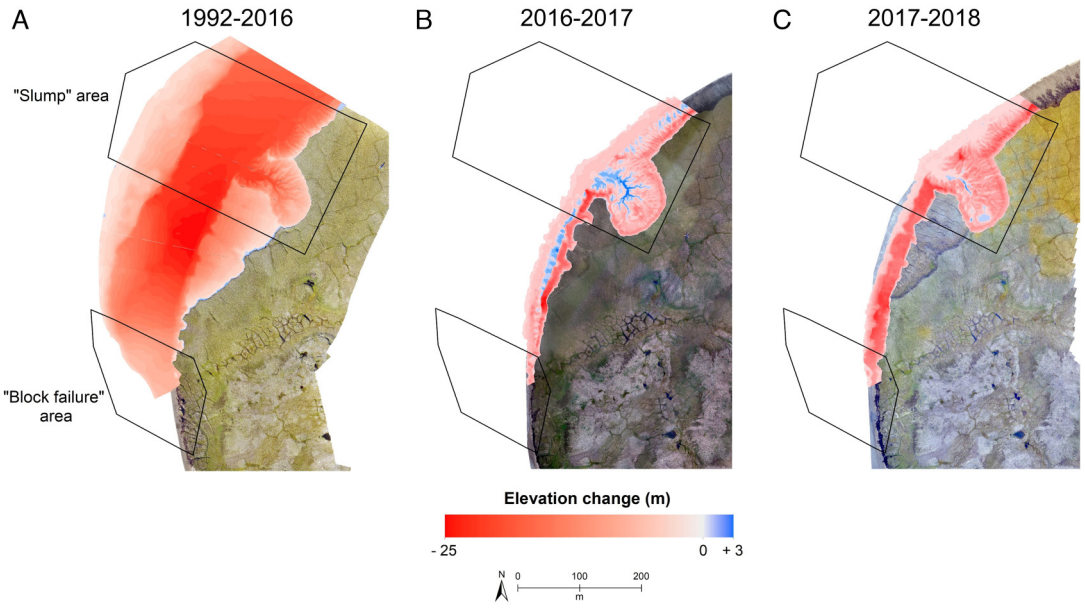

retreat rates in the block failure area remained more consistent through time, whereas the greatest change was in areas experiencing slumping (Fig. 6F).

The mean annual volume change per 100 m of shoreline for each period (1992–2016, 2016–2017, 2017–2018), in each of the block failure and slump areas, is shown along with the mean rates of cliff and shoreline retreat (Fig. 9). Volume change over all time steps was greater in the slump area than the block failure area by an order of magnitude;

Fig. 9. Mean annual volume change per 100 m of shoreline between consecutive digital surface models from 1992, 2016, 2017, and 2018. Mean annual rates of cliff and shoreline retreat are also shown, with error bars of one standard deviation.

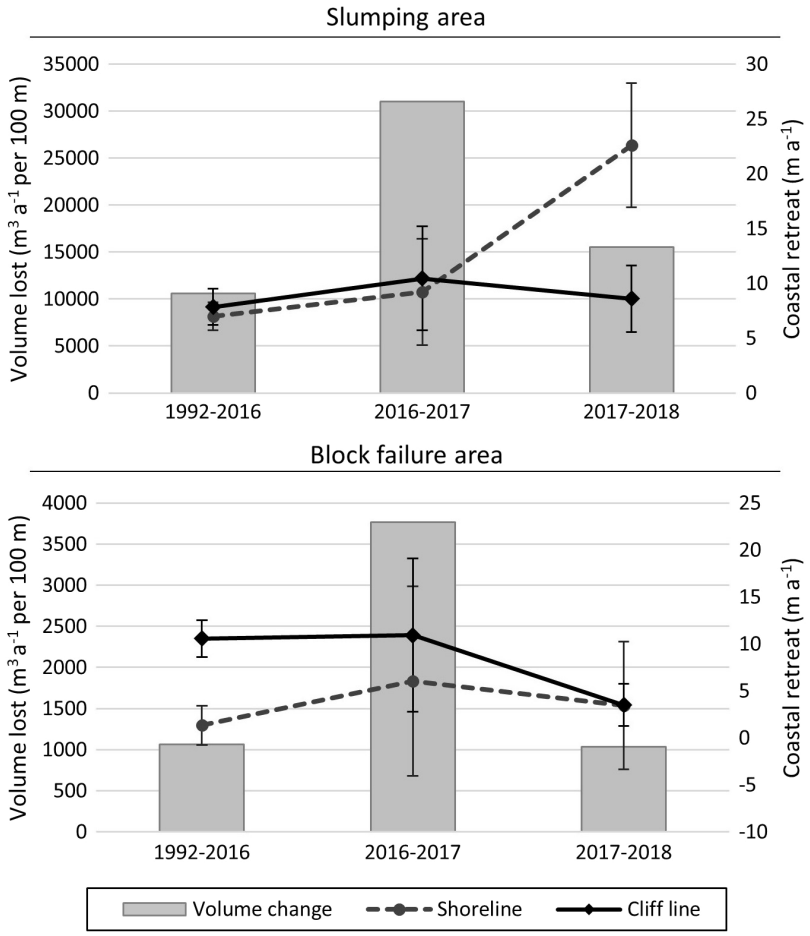

however, the same pattern is shown in both cases, and the greatest change is seen over the 2016–2017 period.

The mean air temperature for July, August, and September recorded at Tuktoyaktuk has been calculated for each year between 1958 and 2018, in addition to a five-year moving average. There is an increasing trend of 3 °C per century (Fig. 10A), with annual variations within ±3 °C of the trendline. Regressions of mean air temperature against rate of cliff retreat (Fig. 10B) reveal a positive, although statistically insignificant correlation across the entire study area ($r^2 = 0.34$; $p = 0.08$), in areas dominated by block failure ($r^2 = 0.08$; $p = 0.5$), and areas dominated by slumping ($r^2 = 0.41$; $p = 0.05$).

The mean annual synoptic and core duration of storms has been identified for the period between 1958 and 2018 (Fig. 10C). Regressions of mean core storm duration against rate of cliff retreat were calculated (Fig. 10D). Positive, but statistically insignificant relationships were found across the entire study area ($r^2 = 0.13$; $p = 0.3$) and in areas dominated by slumping ($r^2 = 0.34$; $p = 0.08$). There is a statistically significant relationship between core storm duration and cliff retreat in the block failure area ($r^2 = 0.84$; $p = 0.0002$).

Fig. 10. (A) Mean July to September air temperature measured at Tuktoyaktuk, Northwest Territories. Note the overall increasing trend (0.03 °C a^{-1}, $r^2 = 0.56$). (B) Mean summer air temperature compared with mean cliff retreat across the entire study area (2.78 m a^{-1} °C^{-1}; $r^2 = 0.34$), the area dominated by slumping (3.90 m a^{-1} °C^{-1}; $r^2 = 0.41$), and the area dominated by block failure (2.90 m a^{-1} °C^{-1}; $r^2 = 0.08$). (C) Mean annual synoptic and core storm duration. Error bars represent one standard deviation from the mean. There is a weak positive trend in synoptic duration (10 min a^{-1}, $r^2 = 0.19$). There is no trend in core storm duration. (D) Mean core storm duration compared with mean cliff retreat across the entire study area (0.22 m a^{-1} h^{-1}; $r^2 = 0.13$), the area dominated by slumping (0.45 m a^{-1} h^{-1}; $r^2 = 0.34$), and the area dominated by block failure (1.84 m a^{-1} h^{-1}; $r^2 = 0.84$).

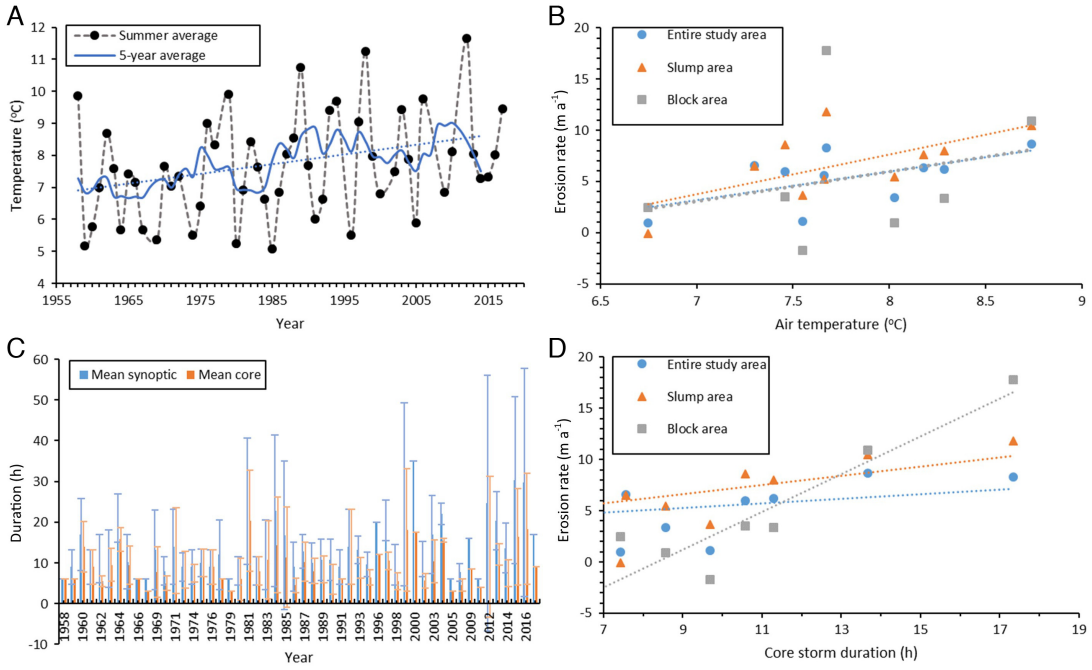

Discussion

The observed rates of cliff and shoreline retreat on Pullen Island (3.4 ± 2.7 and 2.3 ± 3.0 m a^{-1}, respectively) was within one standard deviation of the value of coastal retreat reported by Solomon (2005; see Table 1) for the outer Mackenzie Delta islands (1.5 ± 2.8 m a^{-1}) during comparable time periods (1974–2004 and 1972–2000). Over the entire period of observation (1947–2018), the northwest-facing sections of cliff experienced the most retreat, having lost as much as 330 m over this period and experiencing rates of cliff retreat up to 30 m a^{-1} in some areas. The mean annual rate over the whole study area has increased from 0 to 12 m a^{-1}. The increase in activity is not uniform across the entire cliff; however, the most change is seen around the RTS features, which experienced over 20 m a^{-1} headwall retreat in 2013–2018. Rates of retreat have also increased, although to a lesser degree, in both the non-retrogressive slump sections and block-failure sections (Fig. 7). Indeed, the long-term rates of cliff retreat in the block failure areas and areas of non-retrogressive slumping were primarily between 0 and 5 m a^{-1} between 1947 and 1993. In the following period, 1994–2018, the cliff sections were more variable with regard to rate of retreat; the standard deviation of retreat increased from 3.8 to 6.5 m a^{-1}.

The correlations between retreat rate and both air temperature and core storm duration suggest that both have an influence on cliff retreat. This is in agreement with previous studies relating Arctic coastal erosion to these parameters, including Solomon et al. (1994), who

found that storm intensity was positively correlated with cliff retreat near Tuktoyaktuk and along the Yukon coast, and Günther et al. (2015), who found that summer air temperature was positively correlated with cliff retreat on the Laptev Sea coast. Furthermore, we find that the impacts of air temperature and storm duration seem to have a greater or lesser effect depending on the dominant mechanism of erosion. It appears that warmer years result in more cliff retreat, and more so in the slump areas than block failures. Similarly, years with longer duration of storms tend to experience more cliff retreat, and more so in the areas affected by block failures. This also suggests that, on a broad spatial scale, the decrease in homogeneity of retreat rate appears to be related to different magnitudes of response to environmental change, depending on the primary mechanism of cliff failure for a particular segment of coast.

Block failure responses

Block failure accounts for a small, but annually increasing, section of west-facing cliff. It occurs when the base of the cliff is undercut by waves and thermal erosion, and a whole block of material detaches from the cliff face due to lack of underlying support (Wobus et al. 2011). The occurrence of block failure can be related primarily to the strength and frequency of storms (Baird and Associates 1995), which cause the surges that remove cliff-base sediment and induce thermal erosion at the cliff base. These erosion processes are limited to the open-water season, when sea ice has melted such that waves form and reach the cliff (Aré et al. 2008; Wobus et al. 2011). The two weather components assessed, summer air temperature and storm duration, have positive correlations with block failure. Warmer years are likely to have longer open-water seasons (Goegh-Guldberg et al. 2018), and so have longer periods over which storms may generate waves to cause block failure.

Given the multi-year frequency and variable resolutions of imagery used, assessment of the relationship between weather and cliff retreat assumes that the mean trend effectively represents the mean annual trend. For example, the average number of storms over the time interval represented by the gap between images correlates with the mean retreat rate for that period. However, for much of the study period, it cannot be established whether erosion during the survey-dependent time intervals occurred in the year with the most storms. Cliff change data at the annual resolution are only available for 2016–2018. Over this limited period, however, it was found that the three storms identified between 2016 and 2017 observations had longer core durations and faster wind speeds than the four storms between 2017 and 2018 observations, and that more cliff was lost in the block failure area in the 2016–2017 season. The long-term increasing trends in both summer air temperature and core storm duration suggest that there will be a continued increase in the rate of cliff retreat in the block failure areas in the future.

Slump failure responses

The majority of the surveyed cliff area is eroded primarily through slumping failures, which in permafrost coasts is driven by ground ice melt. This releases previously frozen sediment, removes support for overlying material, and entrains material as the meltwater runs downslope. Generally, the amount of melt depends on the net solar radiation that is received by the ground ice (Lewkowicz 1986). The high-latitude and well-constrained study area means that (a) air temperature is an acceptable generic proxy for solar input, and (b) differences in melt are due to locally defined slope angle and ice exposure, both of which impact net radiation. In principle, higher air temperatures would result in more melt, and thus more rapid headwall retreat; this is supported by the positive correlation between retreat rate and air temperature (Fig. 10B).

There is notable heterogeneity of cliff retreat rates within areas of apparently similar erosion mechanisms, so lateral structural variations must also be considered. The most obvious distinction is between areas with RTSs and those without. Along the northern-most cliffs, slumping occurs, but there is no development of discrete RTS features. In the central cliff section, there are two large, pervasive RTS failures that can be tracked through the study period. The first is currently stable, but over the course of the study period has exhibited several periods of accelerated activity (some time prior to 1947, and for an unknown period between 1992 and 2013 that included 2004) and quiescence (between 1967 and 1985, and again around 2013). The second appears to have initiated around 2013 along the same slope as the former RTS, and retrogressed sufficiently to overtake the original headwall. This "polycyclic" RTS activity, where new slumps initiate on top of older, stabilized slumps, is observed elsewhere in the Beaufort Sea (Lantuit and Pollard 2008). In the transitional and block failure areas small, recurring RTSs have also been observed, which we will refer to as perennial because they develop year after year on the same ground ice body but do not always persist between melt seasons. An exemplar feature of this type is shown in Fig. 11, where the characteristic bowl shape of an RTS, formed by more rapid retreat of the headwall than of the adjacent cliffs, is observed in 2016 and 2018 on what appears to be the same ice wedge exposed in the cliff face. Although the ice wedge is also exposed in 2017, the bowl form is not observed that year, due to the rate of retreat of the adjacent cliffs surpassing the rate of headwall retreat within the feature. Although these small RTSs can form repeatedly on the same ice bodies, if not sufficiently active, then they are destroyed, and the headwall position is reset to the coastal cliff line. In contrast, the larger, persistent RTSs endure between melt seasons and, thus, can progress farther from the headwall position attained the previous year.

The relationship between headwall retreat of an active RTS and meteorological data has been documented in regions near Pullen Island; there is a direct correlation between ablation of exposed ground ice and air temperature (Lewkowicz 1986). Furthermore, there are several known factors that contribute to RTS initiation and maintenance of activity (or, inhibition of stabilization), including size of ice body, slope and ice face angles, and cliff height (Lewkowicz 1986, 1987). Overall, the most important condition of continued RTS activity is that the ice remain exposed; if it becomes covered by sediment due to insufficient slope or melt to remove it, or if the ice body is exhausted, then activity will cease (Burn and Lewkowicz 1990). Exposed ground ice appears to be primarily wedge ice formations, due to the lateral continuity between the ice and the network of polygon on the ground surface. Ice wedge polygon density on the surface appears fairly uniform over the whole slump area, so the lateral differences may cause some variation but would likely even out over longer time scales.

Slope angle is generally steeper outside of RTS structures; however, this is interpreted as a result of the slumps, and not their cause. Based on elevation models, it appears that the slope angle within an RTS decreases over time, whereas the slumping coastal cliffs maintain a more consistent slope angle (Fig. 12). Exposed ground ice has been observed throughout the study area, raising questions about why certain areas develop persistent RTS structures, whereas other areas (with apparently similar structural characteristics and external forces) do not. There are two factors to consider that may play a large role in determining the development of an RTS: cliff height and adjacent cliff behavior.

Broadly speaking, ground materials that are mobilized downslope in an RTS system may come to rest on the headwall, accumulate on the slump floor, or enter the nearshore sediment budget. Lewkowicz (1987) attributed differences in sediment removal to headwall elevation; lower headwalls are more likely to have their ice covered by sediment, impeding ice ablation and halting thaw-related slumping. This is further supported by

Fig. 11. (A) Annotated map of cliff line retreat on a perennial retrogressive thaw slump (RTS), showing development of the characteristic bowl form in 2016, erasure of the feature between 2016 and 2017 observations, and recurrence of the bowl form in 2018. (B) Oblique imagery of the cliff face with the exposed ice wedge indicated, as seen in the 3D models (2016 and 2017) and field photograph (2018). (Imagery courtesy of the Geological Survey of Canada, unpublished data, 2016–2018. Plan view visualized using Esri ArcMap v.10.5, and oblique views using ArcScene v.10.5.).

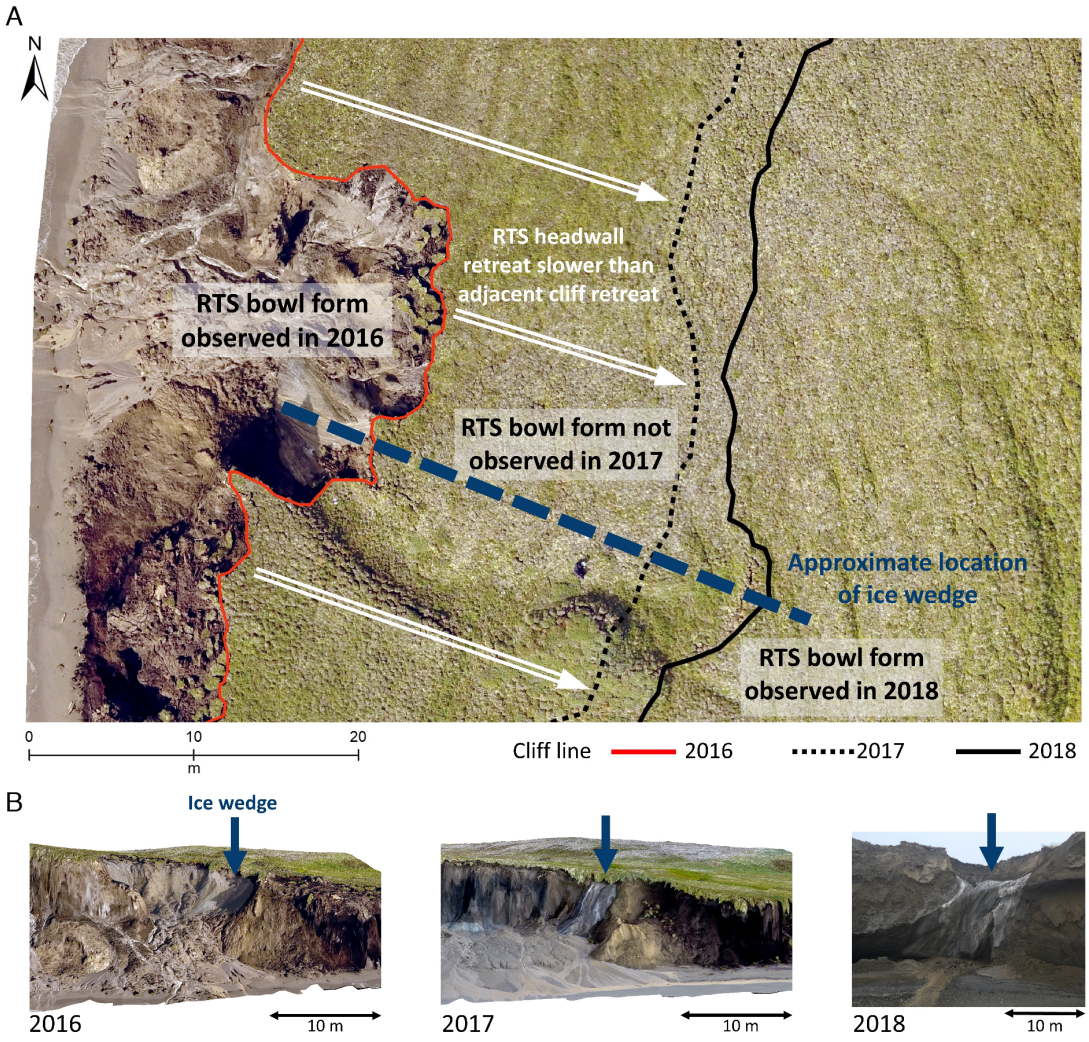

Ramage et al. (2017), who found that coastal RTS activity on the Yukon coast was more likely to occur in areas with higher, steeper cliffs compared with lower or shallower slopes. In the context of our study area, the highest headwall elevations are found in the RTS area, with median elevation 23.5 m. This is followed by the non-RTS slump area, which has a median cliff-top elevation of 18 m. Finally, the block failure area has median cliff-top elevation of 6 m. A possible interpretation is that RTS structures developing in the block failure area tend to have their ice covered efficiently by sediment and subsequently cease activity. Perennial RTSs are observed in the block failure area over successive years, but the adjacent cliff is retreating at such a rate that the characteristic bowl structure is removed before the end of the melt season and loses the positive feedbacks

Fig. 12. Elevation profiles through (1) slumping coastal cliffs, (2) active retrogressive thaw slump, and (3) block failure cliff sections based on photogrammetric digital surface models of Pullen Island in 1992, 2016, 2017, and 2018. Profile locations are shown on oblique view of 1992 imagery (courtesy of Geological Survey of Canada; National Air Photo Library, 1992. Visualized using Esri ArcScene v.10.5.).

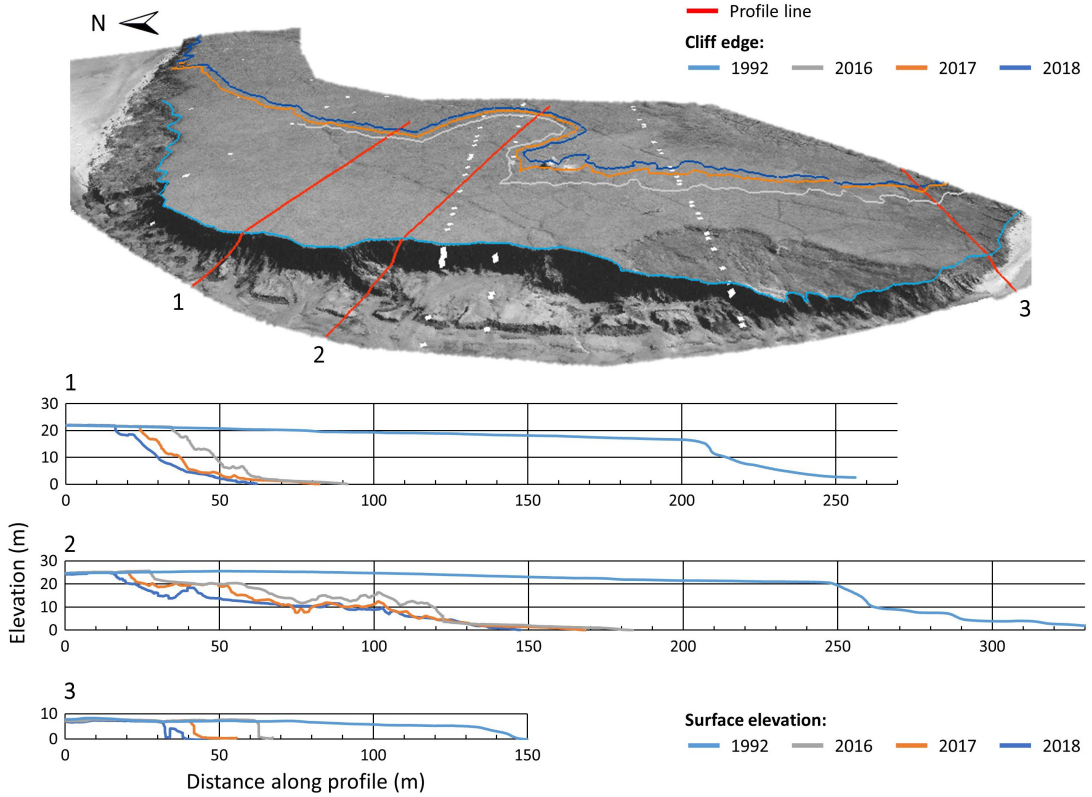

of increased surface area on ablation rate (Lacelle et al. 2015). One determining parameter of the development of a persistent RTS feature is sufficient activity to sustain a more rapid rate of retreat than the adjacent cliff sections. It is perhaps only necessary to maintain this localized elevated rate for a single melt season, such as to establish a bowl-shaped structure of sufficient size that will then begin the following melt season with higher retreat rates than the adjacent cliff. Due to the temporal resolution of the data, this cannot be confirmed for the identified RTS. Given the polycyclic nature of RTSs observed on Pullen Island and elsewhere in coastal (Lantuit and Pollard 2008) and lakeside (Kokelj et al. 2009*a*, 2009*b*) settings, one predictor of RTS activity is prior RTS activity in the region. Considering the history of the study area through the available imagery, it is unlikely that persistent RTS structures such as those seen in the slump area will develop in the block failure area.

Alternative coastal change measurements: shoreline retreat and volume change

Measurements of mean annual retreat of the shoreline (defined here as the base of the slope) yielded similar trends to cliff retreat, being equal within one standard deviation and following the increase in rate over time, although to a lesser degree until the latest period of acceleration (Fig. 6). This would suggest that using either the shore or the cliff line gives an adequate broad sense of coastal change through time, but that at the annual

resolution they are somewhat disconnected from one another, and from measures of volumetric change.

A preliminary statement about the link between shoreline, cliff line, and volumetric changes can be made based on the four DSMs included in this analysis (1992, 2016, 2017, and 2018). When the volumetric change over the block failure and slump areas were calculated from elevation difference between consecutive DSMs, it appears that volume is more directly related to retreat in the block failure area than in the slump area. In the area dominated by block failure, years of greater cliff and shoreline retreat also have greater volume of material lost. In the area affected by slumping, the pattern of volume loss tracks more closely with retreat of the cliff line, although there appears to be a disconnect between volume loss and shoreline retreat; the greatest mean annual volume change of the three periods occurred in 2016–2017, whereas the greatest shoreline retreat occurred in 2017–2018 (Fig. 9).

One potential explanation for the disconnect between shoreline, cliff line, and volume changes are the pathways for eroded material depending on the dominant erosive mechanism. Obu et al. (2016) observed that within their study area on Herschel Island, Yukon, volumetric change was more laterally uniform than planimetric measurements of coastal change, and that some of the short-term variability in coastal retreat was related to a lag between detachment of material from the slope and removal from the shore. In areas being eroded by block failure, material is detached simultaneously from the cliff edge and observable slope base, then removed to the nearshore environment over a period of a couple weeks (Barnhart et al. 2014). It follows, therefore, that planimetric measures of coastal change and loss of material would follow similar trends.

Where the cliff is being eroded by slumping, material is not removed simultaneously from the cliff edge and slope base; sediments may be deposited on the slope, in the base of an RTS, or at the base of the slope, before being removed to the nearshore. Indeed, some net accumulation of sediments is observed within the active RTS in 2016–2017 and 2017–2018 (Figs. 8B and 8C; up to 3 m surface elevation increase). Discrepancies between the amount of material removed from the cliff and from the shore may be the result of redeposition prior to reaching the shore (Obu et al. 2016), volume change due to ice melt (Couture et al. 2018), or due to short-term inconsistencies related to the processes driving sediment movement on the cliff edge (i.e., gravity-driven mobilization) and the slope base (i.e., wave action).

The connections drawn here between volume change and cliff and shoreline retreat on Pullen Island are preliminary due to the inclusion of only three time periods in the analysis. There is some suggestion in the literature that over a sub-annual period there would be more disconnect between cliff and shoreline change, which tend to equilibrate over the course of one or more seasons (Barnhart et al. 2014). The appropriate metric of coastal change likely depends on the application of this value. Net change in volume may be the most representative, if not the most intuitive, metric to apply practically. Adjusting volumetric measurements to account for ice content, thus reporting the change in sediment volume, has been applied to studies of mobilization of carbon, nitrogen, and other soil constituents and impacts on the marine environment (e.g., Couture et al. 2018; Ramage et al. 2018). Changes to shoreline is a commonly used value, and similarly relates to the nearshore sediment budget (e.g., Harper 1978; Solomon 2005). However, for applications regarding terrain loss, impacting terrestrial ecosystems and human land-use and infrastructure, cliff retreat appears to be the most intuitive measurement to report, especially considering the increasing RTS activity across the Canadian Beaufort Sea Coast, and the potential for discrepancy between cliff and shoreline retreat over short periods of time.

Other explanators of coastal retreat

The stratigraphy of Pullen Island is one of the most important factors controlling how rapidly the cliffs are eroding, and their response to other environmental drivers. The ice fraction of eroded material melts and does not become redeposited (Harper et al. 1985), which contributes to the extreme rates of cliff retreat experienced in this area compared with non-permafrost coasts. Limiting sediment as talus prolongs ice exposure and increases local relief (Aré 1988; Kokelj et al. 2015), and leaves the cliff base exposed to thermal and mechanical abrasion (Aré 1988; Baird and Associates 1995).

Slope aspect may also impact cliff retreat as it relates to insolation, which provides the energy to thaw the active layer and sustain RTS activity (Lewkowicz 1986). Variations in aspect within the study area can result in local differences in net radiation (Lewkowicz 1986, 1987). The eroding coasts on Pullen Island range from north-facing in the north of the study area, to west-facing in the south of the study area. Being in the northern hemisphere, the more west-facing slope will receive more direct solar radiation than the north-facing region. However, it is noted that the diffuse sunlight at this latitude and extended polar day mean that the impact is likely not very large compared with other factors that drive coastal retreat (Aré 1988; Wobus et al. 2011). Nonetheless, variation in slope aspect may help to explain, at least in part, the lateral differences in retreat rate of the slumping coastal cliffs in the later years of observation (Fig. 7).

The relationship between failure, transport, and deposition in the nearshore environment is somewhat iterative. The amount of failure determines the volume available to be deposited; this volume decreases when the ice fraction melts. The volume deposited at the base of the slope, in turn, affects the amount of erosion; where there is less sediment available to protect the base of the slope, more rapid removal of material should occur. The balance is maintained by ice content and slope, which influence effective transport; however, these variables are also dependent on the mechanisms of failure and deposition. Changes to one or more of these factors, such as increased air temperatures resulting in more melt or longer open-water seasons and, hence, the susceptibility to wave action, resulting in a change to the other processes in the cycle. Although the finer nuances of these relationships are beyond the scope of this paper, the movement of material and the characteristics (ice content, cliff height, air temperature, etc.,) of the local environment in which it takes place are essential and interdependent controls on the rate of retreat of ice rich permafrost cliffs.

Conclusions

The rate and variability of retreat across the ice-rich cliffs of Pullen Island have increased over the 71 years of observation; the island has gone from a mean annual retreat of <1 m with standard deviation of 2.1 during the 1940s to 1980s, to 12 m a^{-1} retreat with standard deviation of 6.3 in the final five years of the study. The acceleration in retreat is interpreted primarily as a response to increasing air temperatures causing increased ground ice melt. The magnitude of response to air temperature change depends on the dominant erosive mechanism for a particular section of cliff; the slump-dominated cliffs, specifically around the RTS features, accelerated faster than the block failure-dominated sections. The decreasing uniformity of cliff retreat is expected to continue in response to current air temperature trends.

Between 1947 and 2018, Pullen Island experienced cliff line retreat of up to 330 m in some areas, of which up to 50 m retreat occurred between 2013 and 2018. In 2018, the width of the island was approximately 550 m behind the more slowly eroding areas, and between 250 and 500 m behind the more rapidly eroding areas. If the current retreat rate of 12 m a^{-1} is sustained, Pullen Island will cease to exist in its currently recognizable form by the year

2060. Considering the acceleration of retreat that is experienced; however, this may come 10 or 15 years sooner, given the mean long-term acceleration of 0.2 m a^{-1} since 1947, or that of 1.6 m a^{-1} observed between 2013 and 2018.

Both shoreline and cliff line retreat rates are used as measures of coastal change throughout the literature, However, the short-term disconnect between the two metrics may be exacerbated by increased slump activity in the Mackenzie Delta region (Barnhart et al. 2014; Couture et al. 2015). The respective implications for marine and terrestrial impacts of shoreline or cliff line change rates suggests that care should be taken to report the appropriate values depending on their intended application. Where issues of terrain loss are concerned, cliff line retreat appears to be the more intuitive and useful metric of coastal change.

As noted, these conclusions are based on trends of multi-year averages. Future work in this area, with a greater frequency of measurements allowing for annual resolution, will be required to better understand the strength of the relationship between the mechanisms driving cliff retreat and environmental factors. Nevertheless, it is apparent that mechanism-specific magnitudes of response to environmental change contribute to the dynamic complexities of permafrost cliff systems.

Acknowledgements

Funding and support for this project was provided by Natural Resources Canada through the Climate Change Geoscience Program and Polar Continental Shelf Project (PCSP). Additional funding was provided by the Inuvialuit Regional Corporation (IRC) and Crown-Indigenous Relations and Northern Affairs Canada (CIRNAC) through the Beaufort Sea Regional Strategic Environment and Research Assessment (BRSEA). In addition, this work was made possible through the Natural Environment and Research Council (NERC) sponsored UK-Canada Arctic bursary program. We are grateful to the field crews, in particular Paul Fraser, Angus Robertson, Roger Macleod from Natural Resources Canada (NRCan), and Andrew Clark from the University of Calgary for acquiring the unmanned aerial vehicle (UAV) data used in this study. We would also like to acknowledge the Aurora Research Institute (ARI), the Inuvialuit Game Council, and the communities and Hunters and Trappers Committees of Inuvik and Tuktoyaktuk for their continued support.

References

Aré, F.E., 1988. Thermal abrasion of sea coasts (part I). Polar Geogr. Geol. **12**(1): 1. doi: 10.1080/10889378809377343.

Aré, F., Reimnitz, E., Grigoriev, M., Hubberten, H.-W., and Rachold, V., 2008. The influence of cryogenic processes on the erosional Arctic shoreface. J. Coast. Res. **241**(1): 110–121. doi: 10.2112/05-0573.1.

Atkinson, D.E., 2005. Observed storminess patterns and trends in the circum-Arctic coastal regime. Geo-Mar. Lett. **25**(2): 98–109. doi: 10.1007/s00367-004-0191-0.

Baird, W.F., and Associates. 1995. Development of a model for the thermal-mechanical erosion on arctic coasts. Final report prepared for Geological Survey of Canada, Oakville, Ontario, Canada.

Barnhart, K.R., Anderson, R.S., Overeem, I., Wobus, C., Clow, G.D., and Urban, F.E., 2014. Modeling erosion of ice-rich permafrost bluffs along the Alaskan Beaufort Sea coast. J. Geophys. Res.: Earth Surf. **119**(5): 1155–1179. doi: 10.1002/2013jf002845.

Boak, E.H., and Turner, I.L., 2005. Shoreline definition and detection: a review. J. Coast. Res. **214**: 688–703. doi: 10.2112/03-0071.1.

Burn, C.R., and Lewkowicz, A.G., 1990. Retrogressive thaw slumps. Can. Geogr. **34**: 273–276. doi: 10.1111/j.1541-0064.1990.tb01092.x.

Cassidy, A.E., Christen, A., and Henry, G.H.R., 2016. The effect of a permafrost disturbance on growing-season carbon dioxide fluxes in a high Arctic tundra ecosystem. J. Geophys. Res. Biogeosci. **13**: 2291–230. doi: 10.5194/bg-13-2291-2016.

Cunliffe, A.M., Tanski, G., Radosavljevic, B., Palmer, W.F., Sachs, T., Lantuit, H., et al. 2019. Rapid retreat of permafrost coastline observed with aerial drone photogrammetry. Cryosphere, **13**: 1513–1528. doi: 10.5194/tc-13-1513-2019.

Couture, N.J., Forbes, D.L., Fraser, P.R., Frobel, D., Jenner, K.A., Manson, G.K., et al. 2015. A coastal information system for the southeastern Beaufort Sea, Yukon and Northwest Territories. Geological Survey of Canada, Open File 7778. doi: 10.4095/295975.

Couture, N.J., Irrgang, A., Pollard, W., Lantuit, H., and Fritz, M., 2018. Coastal erosion of permafrost soils along the Yukon Coastal Plain and fluxes of organic carbon to the Canadian Beaufort Sea. J. Geophys. Res. Biogeosci. **123**(2): 406–422. doi: 10.1002/2017JG004166.

Dallimore, S.R., Wolfe, S.A., and Solomon, S.M., 1996. Influence of ground ice and permafrost on coastal evolution, Richards Island, Beaufort Sea coast, N.W.T. Can. J. Earth Sci. **33**: 664–675. doi: 10.1139/e96-050.

Environment Canada, 2014. Coastal and nearshore bird usage of the Canadian Beaufort Sea. Data prepared by the Canadian Wildlife Service (CWS) and Upon-LGL Limited.

Environment and Climate Change Canada. 2016. Hourly data (Jul 2016) – Climate ID 2203911 – Tuktoyaktuk A, Northwest Territories [Table]. Available from https://climate.weather.gc.ca/historical_data/search_historic_data_e.html.

Galley, R.J., Else, B.G.T., Howell, S.E.L., Lukovich, J.V., and Barber, D.G., 2012. Landfast sea ice conditions in the Canadian Arctic: 1983–2009. Arctic, **65**(2): 133–144. doi: 10.14430/arctic4195.

Goegh-Guldberg, O.D., Jacob, D., Taylor, M., Bindi, M., Brown, S., Camilloni, I., et al. 2018. Impacts of 1.5 °C global warming on natural and human systems. *In* Global warming of 1.5°C. An IPCC Special Report on the impacts of global warming of 1.5°C above pre-industrial levels and related global greenhouse gas emission pathways in the context of strengthening the global response to the threat of climate change, sustainable development, and efforts to eradicate poverty. *Edited by* V. Masson-Delmotte, V. Zhai, P. Portner, H.-O. Roberts, D. Skea, J. Shukla et al.

Günther, F., Overduin, P.P., Yakshina, I.A., Opel, T., Baranskaya, A.V., and Grigoriev, M.N. 2015. Observing Muostakh disappear: permafrost thaw subsidence and erosion of a ground-ice-rich island in response to arctic summer warming and sea ice reduction. Cryosphere, **9**(1): 151–178. doi: 10.5194/tc-9-151-2015.

Harper, J.R., 1978. Coastal erosion rates along the Chukchi Sea coast near Barrow, Alaska. Arctic, **31**(4): 428–433. doi: 10.14430/arctic2670.

Harper, J.R. 1990. Morphology of the Canadian Beaufort Sea Coast. *In* The Beaufort Sea coastal zone. *Edited by* P.R. Hill. Marine Geology. pp. 75–91.

Harper, J.R., Reimer, P.D., and Collins, A.D., 1985. Canadian Beaufort Sea: physical shore-zone analysis. Geological Survey of Canada, Open File 1689: p. 105.

Hugelius, G., Strauss, J., Zubrzycki, S., Harden, J.W., Schuur, E.A.G., Ping, C.-L., et al. 2014. Estimated stocks of circumpolar permafrost carbon with quantified uncertainty ranges and identified data gaps. J. Geophys. Res. Biogeosci. **11**: 6573–6593. doi: 10.5194/bg-11-6573-2014.

Kokelj, S.V., and GeoNorth Ltd. 2002. Drilling mud sumps in the Mackenzie Delta Region: construction, abandonment and past performance. Report to the Department of Indian Affairs and Northern Development, Northwest Territories Region. 16 pp.

Kokelj, S.V., Lantz, T.C., Kanigan, J., Smith, S.L., and Coutts, R. 2009*a*. Origin and polycyclic behaviour of tundra thaw slumps, Mackenzie Delta region, Northwest Territories, Canada. Permafr. Periglac. Process. **20**(2): 173–184. doi: 10.1002/ppp.642.

Kokelj, S.V., Zaidlik, B., and Thompson, M.S. 2009*b*. The impacts of thawing permafrost on the chemistry of lakes across the subarctic boreal-tundra transition, Mackenzie Delta region, Canada. Permafr. Periglac. Process. **20**: 185–199. doi: 10.1002/ppp.641.

Kokelj, S.V., Tunnicliffe, J., Lacelle, D., Lantz, T.C., Chin, K.S., and Fraser, R. 2015. Increased precipitation drives mega slump development and destabilization of ice-rich permafrost terrain, northwest Canada. Glob. Planet. Change, **129**: 56–68. doi: 10.1016/j.gloplacha.2015.02.008.

Lacelle, D., Brooker, A., Fraser, R.H., and Kokelj, S.V., 2015. Distribution and growth of thaw slumps in the Richardson Mountains-Peel Plateau region, northwestern Canada. Geomorphology, **235**: 40–51. doi: 10.1016/j.geomorph.2015.01.024.

Lantuit, H., and Pollard, W.H., 2005. Temporal stereogrammetric analysis of retrogressive thaw slumps on Herschel Island, Yukon Territory. Nat. Hazards Earth Syst. Sci. **5**: 413–423. doi: 10.5194/nhess-5-413-2005.

Lantuit, H., and Pollard, W.H., 2008. Fifty years of coastal erosion and retrogressive thaw slump activity on Herschel Island, Southern Beaufort Sea, Yukon Territory, Canada. Geomorphology, **95**(1): 84–102. doi: 10.1016/j.geomorph.2006.07.040.

Lewkowicz, A.G., 1986. Rate of short-term ablation of exposed ground ice, Banks Island, Northwest Territories, Canada. J. Glaciol. **32**(112): 511–519. doi: 10.1017/S0022143000012223.

Lewkowicz, A.G., 1987. Headwall retreat of ground-ice slumps, Banks Island, Northwest Territories. Can. J. Earth Sci. **24**: 1077–1087. doi: 10.1139/e87-105.

Mackay, J.R., 1986. Fifty years of coastal retreat west of Tuktoyaktuk, District of Mackenzie. Current Research, Part A, Geological Survey of Canada, Paper 86-1A. pp. 727–735. doi: 10.4095/120445.

Mackay, J.R., 1972. The world of underground ice. Ann. Am. Assoc. Geogr. **62**(1): 1–22. doi: 10.1111/j.1467-8306.1972.tb00839.x.

Manson, G.K., and Solomon, S.M., 2007. Past and future forcing of Beaufort Sea coastal change. Atmos. Ocean, **45**(2): 107–122. doi: 10.3137/ao.450204.

Mahoney, A.R. 2018. Landfast sea ice in a changing arctic. *In* Arctic Report Card 2018. *Edited by* E. Osborne, J. Richter-Menge, and M. Jeffries. 2018. www.arctic.noaa.gov/Report-Card.

Murton, J.B., Waller, R.I., Hart, J.K., Whiteman, C.A., Pollard, W.H., and Clark, I.D. 2004. Stratigraphy and glaciotectonic structures of permafrost deformed beneath the northwest margin of the Laurentide Ice Sheet, Tuktoyaktuk Coastlands, Canada. J. Glaciol. **50**(170): 399–412. doi: 10.3189/172756504781829927.

National Air Photo Library. 1992. Aerial photographs of Pullen Island, Northwest Territories. 1:6000. Roll Number A28263, Photo Numbers 0248-0251; 0261-0265 [Photographs]. Available from https://www.eodms-sgdot.nrcan-rncan.gc.ca.

Obu, J., Lantuit, H., Fritz, M., Pollard, W.H., Sachs, T., and Günther, F., 2016. Relation between planimetric and volumetric measurements of permafrost coast erosion: a case study from Herschel Island, western Canadian Arctic. Polar Res. **35**(1): 30313. doi: 10.3402/polar.v35.30313.

Rachold, V., Grigoriev, M.N., Aré, F.E., Solomon, S., Reimnitz, E., Kassens, H., and Antonow, M, 2000. Coastal erosion vs riverine sediment discharge in the Arctic Shelf seas. Int. J. Earth Sci. **89**(3): 450–460. doi: 10.1007/s005310000113.

Radosavljevic, B., Lantuit, H., Pollard, W., Overduin, P., Couture, N., Sachs, T., et al. 2016. Erosion and flooding — threats to coastal infrastructure in the Arctic: a case study from Herschel Island, Yukon Territory, Canada. Estuar. Coasts, **39**(4): 900–915. doi: 10.1007/s12237-015-0046-0.

Ramage, J.L., Irrgang, A.M., Herzchuh, U., Morgerstern, A., Couture, N., and Lantuit, H. 2017. Terrain controls on the occurrence of coastal retrogressive thaw slumps along the Yukon Coast, Canada. J. Geophys. Res. Earth Surf. **122**: 1619–1634. doi: 10.1002/2017JF004231.

Ramage, J.L., Irrgang, A.M., Morgerstern, A., Couture, N., and Lantuit, H., 2018. Increasing coastal slump activity impacts the release of sediment and organic carbon into the Arctic Ocean. J. Geophys. Res. Biogeosci. **15**: 1483–1495. doi: 10.5194/bg-15-1483-2018.

Solomon, S.M., 2005. Spatial and temporal variability of shoreline change in the Beaufort-Mackenzie region, Northwest Territories, Canada. Geo-Mar. Lett. **25**: 127–137. doi: 10.1007/s00367-004-0194-x.

Solomon, S.M., Forbes, D.L., and Kierstead, B., 1994. Coastal impacts of climate change: Beaufort Sea erosion study. Geological Survey of Canada, Open File 2890. 85 p. doi: 10.4095/194148.

Statistics Canada. 2016*a*. 2016 Census — boundary files: lakes and rivers (polygons), cartographic boundary file [shapefile]. Statistics Canada Catalogue.

Statistics Canada. 2016*b*. 2016 Census — boundary files: provinces/territories, water file [shapefile]. Statistics Canada Catalogue.

Tanski, G., Lantuit, H., Ruttor, S., Knoblauch, C., Radosavljevic, B., Strauss, J., et al. 2017. Transformation of terrestrial organic matter along thermokarst-affected permafrost coasts in the Arctic. Sci. Total Environ. **581**: 434–447. doi: 10.1016/j.scitotenv.2016.12.152.

Taylor, A.E., Dallimore, S.R., and Judge, A.S., 1996. Late Quaternary history of the Mackenzie-Beaufort region, Arctic Canada, from modelling of permafrost temperatures. 2. The Mackenzie Delta — Tuktoyaktuk Coastlands. Can. J. Earth Sci. **33**(1): 62–71. doi: 10.1139/e96-007.

Thieler, E.R., Himmelstoss, E.A., Zichichi, J.L., and Ergul, A., 2017. The Digital Shoreline Analysis System (DSAS) Version 4.0 — an ArcGIS extension for calculating shoreline change. U.S. Geological Survey Open-File Report 2008-1278.

Ullman, S. 1977. The interpretation of visual motion. Ph.D. thesis, Massachusetts Institute of Technology, Department of Electrical Engineering and Computer Science.

Ullman, S. 1979. The interpretation of structure from motion. Proc. Royal Soc. B, **203**(1153): 405–426. doi: 10.1098/rspb.1979.0006.

Wobus, C., Anderson, R., Overeem, I., Matell, N., Clow, G., and Urban, F. 2011. Thermal erosion of a permafrost coastline: improving process based models using time-lapse photography. Arct. Antarct. Alp. Res. **43**(3): 474–484. doi: 10.1657/1938-4246-43.3.474.